Direct transition to electroconvection in a homeotropic nematic liquid crystal

4 **AUTHORS**, INCLUDING:

Agnes Buka
Hungarian Academy of Sciences
111 PUBLICATIONS **1,348** CITATIONS

Werner Pesch
University of Bayreuth
135 PUBLICATIONS **2,536** CITATIONS

Direct transition to electroconvection in a homeotropic nematic liquid crystal

Á. Buka

*Research Institute for Solid State Physics and Optics, Hungarian Academy of Sciences,
P.O. Box 49, H-1525 Budapest, Hungary*

B. Dressel, L. Kramer, and W. Pesch[a)]

Physikalisches Institut, Universität Bayreuth, D-95440 Bayreuth, Germany

We present an experimental and theoretical investigation of a variant of electroconvection using an unusual nematic liquid crystal in an isotropic configuration (homeotropic alignment). The significance of the system is a direct transition to the convecting state due to the negative conductivity anisotropy and positive dielectric anisotropy. We observe at onset rolls or squares depending on the frequency and amplitude of the applied ac voltage with a strong signature of the zigzag instability. Good agreement with calculations based on the underlying hydrodynamic theory is found. We also construct an extended Swift–Hohenberg model which allows us to capture complex patterns like squares with a quasiperiodic modulation. © *2004 American Institute of Physics.* [DOI: 10.1063/1.1774412]

Nonequilibrium transitions in spatially extended continuum systems lead to a wide variety of fascinating patterns. The basic elements are stripes (or rolls), squares, and (under some restrictions) hexagons, which are the only simple *periodic* patterns that appear directly via a supercritical bifurcation in isotropic quasi-two-dimensional systems.[1] In rare cases there is a direct (supercritical) transition to a *disordered state* and/or to *spatial-temporal chaos*. Here we study electroconvection (EC) in an unusual nematic liquid crystal with strongly positive dielectric anisotropy and negative anisotropy of the conductivity. This unusual combination of the material parameters leads in the isotropic configuration (homeotropic alignment) to a direct transition into rolls and/or squares which in most cases show a characteristic disorder and are well described by the theory. We perform a linear and nonlinear analysis of the full nemato-hydrodynamic equations and carry out simulations of a suitably constructed Swift−Hohenberg model. We obtain, in agreement with the experiments modulated rolls and squares at threshold. The type of modulation is of disordered zigzag in the roll regime and undulated for the squares. The square undulations are initially irregular and after a long time they become almost periodic. For some class of parameters and initial conditions in simulations the undulations become completely regular and the structure locks into a static, spatially quasiperiodic attractor. To our knowledge a direct transition to a quasiperiodic pattern with square symmetry has never been discussed.

I. INTRODUCTION

Nematic liquid crystals, the simplest type of intrinsically anisotropic fluids, continue to provide model systems for a wide variety of interesting nonlinear dynamical phenomena like optical instabilities,[2] flow-induced nonlinear waves,[3] critical properties of nonequilibrium transitions,[4] and in particular electrically or thermally driven convection instabilities.[5] Whereas convection in nematics has so far contributed substantially to our general understanding of anisotropic pattern-forming systems we present here in particular a direct transition to *isotropic convection* which opens up scenarios unaccessible in simple fluids.

In nematics the mean orientation of the rodlike molecules is described by the director $\hat{\mathbf{n}}$. The uniaxial anisotropy is reflected in the material parameters such as the electric conductivity tensor $\sigma_{ij} = \sigma_\perp \delta_{ij} + \sigma_a n_i n_j$ where $\sigma_a = \sigma_\parallel - \sigma_\perp$ (and analogously the dielectric permittivity ϵ_{ij}). Here $\sigma_\parallel$, $\sigma_\perp$ are the conductivities parallel and perpendicular to $\hat{\mathbf{n}}$, respectively.[6] Electroconvection (EC) is driven in a nematic layer by an ac voltage (effective amplitude U, frequency $\omega = 2\pi f$) applied between two bounding plates. Commonly the *planar* configuration is considered, where the uniaxial anisotropy is externally expressed by anchoring the director along an axis parallel to the plates. Typically one chooses materials like 4-methoxybenzylidene-4′-*n*-butyl-aniline (MBBA)[7] with negative dielectric anisotropy ($\epsilon_a = \epsilon_\parallel - \epsilon_\perp < 0$) and positive conductivity anisotropy ($\sigma_a > 0$) where one obtains a satisfactory overall theoretical description.[8,9] In this paper we focus on EC in a *homeotropically* aligned (no external anisotropy is imposed) nematic with the unusual combination of $\sigma_a < 0$ and $\epsilon_a > 0$. Whereas the possibility of a direct transition to EC in this case has been anticipated in the early literature,[6] the experimental study has started only recently.[10] Depending on ω one finds transitions to rolls or squares at onset with random global orientation. The patterns exhibit spatial modulations with a slow dynamics (see Figs. 1–4, to be discussed below).

The quantitative analysis of our experimental results is first based on the standard nematohydrodynamic equations (NHDE). In this framework even the linear stability analysis

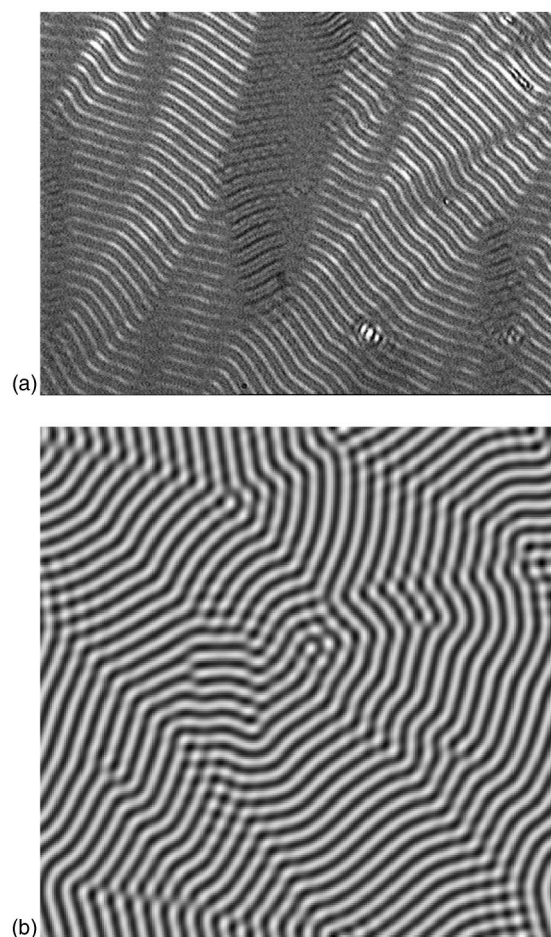[a)]Electronic mail: werner.pesch@uni-bayreuth.de

FIG. 1. Snapshots of ZZ roll patterns in experiment (a) ($\varepsilon = 0.038$, $\omega/\omega_{\mathrm{exp}}^* = 0.18$) and in simulation (b) of the SH-equation ($\varepsilon = 0.006$, $\omega/\omega_{\mathrm{theo}}^* = 0.16$).

FIG. 2. Snapshots of rolls+squares in experiment (a) ($\varepsilon = 0.08$, $\omega/\omega_{\mathrm{exp}}^* = 0.65$) and in simulation (b) of the SH-equation ($\varepsilon = 0.01$, $\omega/\omega_{\mathrm{theo}}^* = 0.74$).

of the uniform homeotropic ground state requires already, if done rigorously, extensive numerics, not to mention the much more difficult nonlinear regime. A much better insight into pattern formation near threshold is provided by universal amplitude and order parameter equations, whose form is governed by the symmetries of the problem, while largely independent of physical details.[11,12] The underlying concepts have been mainly developed and tested in Rayleigh–Bénard convection (RBC) driven by a temperature gradient in a horizontal layer of a simple fluid.[1,11,13] The competition between the prevailing stripes (rolls) and hexagons near threshold is well understood after the pioneering work of Busse in RBC.[14] Although squares are observed in quite diverse systems[15] studies of their nonlinear aspects are scarce.[19] To assess the complex patterns found in our experiments we have constructed on the basis of the NHDE results suitably chosen amplitude equations and their isotropic generalization (Swift–Hohenberg model), which describe the experiments near threshold very well.

The paper includes a brief review on general concepts and of results presented elsewhere.[10,20] It is organized as follows: In Sec. II we describe the experimental background of our system and present the typical patterns. Section III is devoted to the onset of convection. A discussion of the main ingredients of the destabilization mechanism of the homeo-
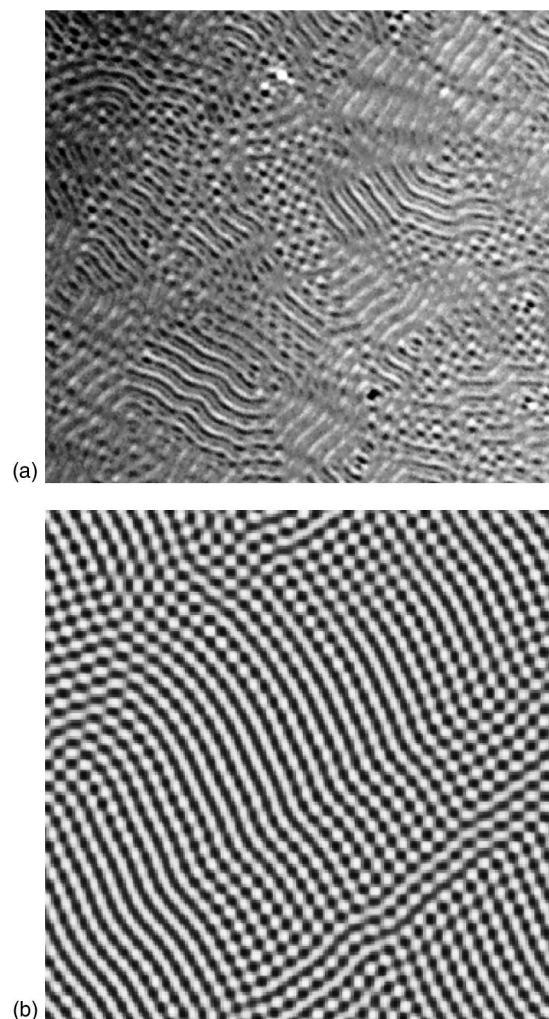
tropic ground state is included. The comparison between the rigorous linear stability analysis and the experiments allows us to extract some unknown material parameters of our nematic. In Sec. IV the stability of patterns in the nonlinear regime is discussed. This leads naturally to the construction of the appropriate Swift–Hohenberg equations (SHE). Section V deals with a discussion of results from numerical simulations of the SHE. The paper ends with some conclusions and general remarks in Sec. VI.

II. EXPERIMENT

The material used in the experiments was p-(nitrobenzyloxy)biphenyl,[21] which shows a nematic phase in the temperature range from $T = 110$ to $94\,°C$, where a transition to a smectic phase takes place.[22] Presumably the critical fluctuations associated with the continuous transition from the smectic C (S_c) to the nematic phase are responsible for the negative conductivity anisotropy $\sigma_a < 0$ in the whole nematic range. Some material parameters such as the dielectric susceptibilities ($\epsilon_\parallel$ and $\epsilon_\perp$), the conductivities ($\sigma_\parallel$ and $\sigma_\perp$) and one of the elastic constants K_{11} have been measured as a function of temperature.
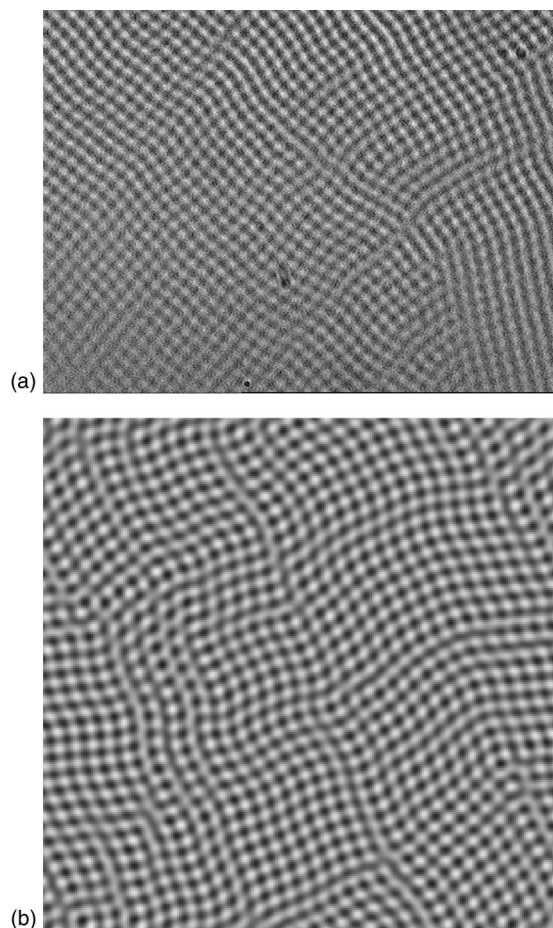
(a)

(b)

FIG. 3. Snapshots of soft squares slightly above ω^* in experiment (a) ($\varepsilon = 0.038$, $\omega/\omega^*_{exp}=1.16$) and in simulations (b) of the SH-equation ($\varepsilon = 0.022$, $\omega/\omega^*_{theo}=1.07$).

(a)

(b)

FIG. 4. Snapshots of "soft" square patterns with same parameter as in Fig. 3, but at a later stage.

EC measurements have been carried out in the nematic range at 96 °C. The temperature was controlled in an Instec hotstage with an accuracy of 0.05 °C. Cells with homeotropic alignment have been prepared with the nematic layer of thickness $d=11\pm1$ μm sandwiched between SnO$_2$ coated float glass plates (in the xy plane) used as electrodes to apply the electric voltage across the sample (in the z direction). The patterns have been observed in a polarizing microscope and recorded by a charge-coupled device (CCD) camera connected to a frame grabber card. Images have been digitized with a spatial resolution of 512×512 pixels and 256 gray-scales.

For the *homeotropic alignment*, where the director is anchored perpendicular to the bounding electrodes (i.e., parallel to the applied voltage), EC sets in directly from the undistorted state via a supercritical bifurcation in the whole conductive range up to its upper limit at the cutoff frequency ω_{cut}. We found $\omega_{cut}\tau_q=0.7$ with the charge relaxation time $\tau_q=\epsilon_\perp/\sigma_\perp$. Note that, in the standard materials ($\epsilon_a<0,\sigma_a >0$) a homogeneous director distortion (a Freedericks transition) precedes the transition to EHC which changes the situation completely[23] (see also Ref. 10 and further references therein).

For low frequencies we observe at threshold a pattern of rolls (stripes) broken up into different domains [see Fig.
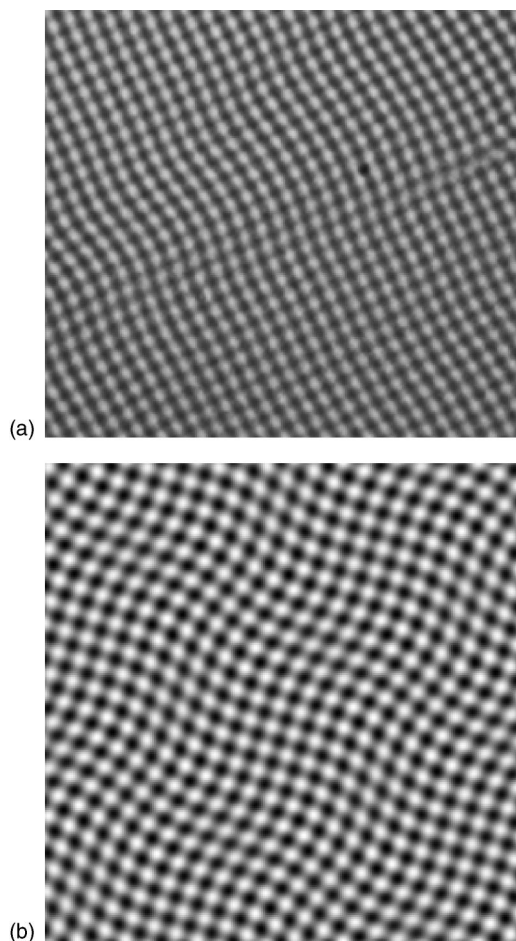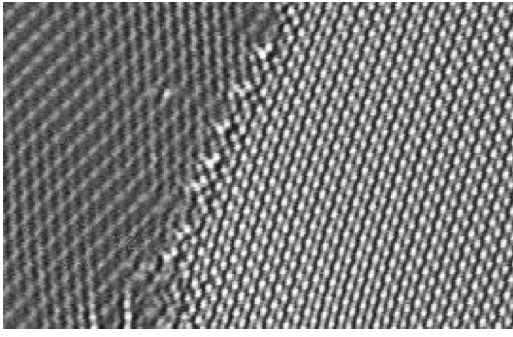
1(a)]. In most cases the roll orientation changes abruptly at the domain walls, which is typical for the zigzag (ZZ) instability driven by pure transverse modulations of rolls. The in-plane director (projection of the director onto the xy plane) is found experimentally to be perpendicular to the (local) roll direction. The difference in brightness and contrast in the different domains of Fig. 1(a) is of purely optical origin depending on the local angle between the director and the polarizer. Although the ZZ instability is characteristic for isotropic systems this type of structure can rarely be observed in other systems under quasistationary conditions (see the discussion below). There is persistent slow dynamics.

Occasionally rolls at different angles form overlap regions of rectangularlike patterns. Their area grows at the expense of the uniform stripe patches with increasing frequency. In an intermediate frequency range extended patches of rolls and squares (R+S, a mixture of the two patterns) appear [see Fig. 2(a)] and above a critical frequency ω^*_{exp} with $\omega^*_{exp}\tau_q=0.56$ all stripe regions have disappeared. The resulting square patterns retain near threshold some features of the ZZ character of the stripes, i.e., the lines making up the squares are undulated. We call this structure *soft square* pattern. In Fig. 3(a) we show a typical example at an early stage of the experiment where in addition to the ZZ modulation one has defect lines. It needs a relaxation time t_r,

FIG. 5. Snapshot of hard squares at $\omega\tau_q = 0.53$ and $\varepsilon = 0.81$.

FIG. 6. Sketch of a convection roll for homeotropic alignment in the x,z-plane ($\lambda = 2\pi/q$): velocity field (short dashed), and director field $\mathbf{n} = (n_x, 0, n_z)$ for experimental material parameters. Also indicated is the space charge distribution at a time where the electric field points upward (otherwise the signs are exchanged).

which is typically about a quarter of an hour, to reach the steady state with nearly defect free regions and extremely slow dynamics, see Fig. 4(a). t_r is of the order $10^4\tau_d$. Since the director relaxation time τ_d[6,8] sets the scale for the local dynamics, t_r corresponds to the diffusion time over a horizontal distance of 100 coherence lenghts, which corresponds to roughly 100 rolls. Note that τ_d is comparable to the characteristic Ginzburg–Landau time τ_0 introduced in Sec. IV below.

Penetrating into the nonlinear regime (increasing the voltage further above threshold) we observe at low frequencies in the ZZ regime a persistent decrease of the size of the patches with uniform roll orientation and acceleration of the dynamics. Thus the patterns look eventually spatiotemporally chaotic, but without the point defects typical for anisotropic convection. At high frequencies (above ω^*_{exp} already at rather small ϵ), on the other hand, the soft square patterns first undergo a transition ending in crystal-like, rigid, almost perfect, quadratic, or slightly rhombic lattices with sharp boundaries between differently oriented domains (see Fig. 5). We call them *hard square* patterns. Hard-square domains coarsen with time and do not qualitatively change with the voltage up to a critical value where they undergo a discontinuous transition to spatio-temporal chaos. The hard-square patterns occur also below ω^*_{exp} (at larger ε) down to $\omega\tau_q = 0.34$ where their transition line merges with the onset of spatio-temporal chaos.
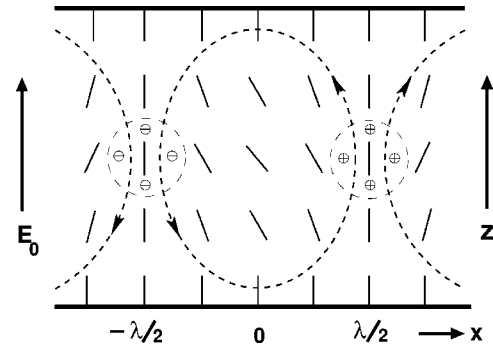
III. THRESHOLD BEHAVIOR

First we discuss the qualitative features of the basic (Carr–Helfrich) destabilization mechanism operative in our material on the basis of the NHDE, which consist of the generalized incompressible Navier–Stokes equation, the rate equation for the director field $\hat{\mathbf{n}}$ ("torque balance") and the quasistatic Maxwell equations, i.e., the Poisson and charge conservation equations[6]

$$\nabla(\boldsymbol{\epsilon}\cdot\mathbf{E}) = \rho_{el}, \quad \nabla(\boldsymbol{\sigma}\cdot\mathbf{E}) = -\partial_t\rho_{el}, \tag{1}$$

with the electric field $\mathbf{E}$ and the electric charge density ρ_{el}.

Consider a (small) director fluctuation $\delta\mathbf{n} = (n_x, 0, 1 - n_x^2/2)$ where the planar perturbation about the homeotropic ground state $\mathbf{n}_0 = \hat{z}$ is given as $n_x = -n_{x0}\cos(qx)\cos(\pi z/d)$, see Fig. 6. Note that the assumption of spatial variations only in the x-, z-plane is not a restriction in our isotropic system. The director distortion modifies the permittivity and conduc-

tivity tensors and leads in the presence of the applied electric field $\mathbf{E}_0 = E_0\hat{\mathbf{z}}\cos(\omega t)$, with $E_0 = \sqrt{2}(U/d)$, via Eq. (1) to space charges ("charge focusing mechanism") and thus to a deformation of $\mathbf{E}_0$ in the form $\delta\mathbf{E} = -\nabla\phi$ with the electric potential ϕ. After elimination of ϕ one obtains for the in-phase component of the charge density [the component $\sim\sin(\omega t)$ is not needed below]

$$\rho_{el}(x,z,t) = Q(q',\omega')qn_{x0}\sin(qx)$$
$$\times\cos(\pi z/d)\cos(\omega t)\epsilon_\perp E_0, \tag{2}$$

where

$$Q(q',\omega') = -(\sigma'_a - \epsilon'_a)\frac{\sigma(q')(1+q'^2)}{\sigma(q')^2 + \omega'^2\epsilon(q')^2}, \tag{3}$$

$$\epsilon(q') = 1 + \epsilon'_a + q'^2, \quad \sigma(q') = 1 + \sigma'_a + q'^2, \tag{4}$$

with the dimensionless quantities $q' = qd/\pi$, $\omega' = \omega\tau_q$, $\sigma'_a = \sigma_a/\sigma_\perp$, $\epsilon'_a = \epsilon_a/\epsilon_\perp$. For our material the Helfrich parameter $\sigma'_a - \epsilon'_a$ is negative, i.e., $Q > 0$. The space charge density ρ_{el} (2) is indicated in Fig. 6. The resulting flow field $\mathbf{v} = (v_x, 0, v_z)$ generated in the Navier–Stokes equations by the Coulomb force $1/2\overline{\rho_{el}E_0}$ (the factor 1/2 arises from the time average denoted by the overbar) is also illustrated in Fig. 6. Note that $\mathbf{v}$ and $\hat{\mathbf{n}}$ are here constant in time in contrast to the time periodic fields ϕ and ρ_{el}. The velocity field $\mathbf{v}$ then acts back on the director via the viscous torques $\Gamma_y = \Gamma_2 + \Gamma_3$ where $\Gamma_2 = -\alpha_2\partial_z v_x$, $\Gamma_3 = -\alpha_3\partial_x v_z \sim \alpha_3 q'^2(d/\pi)v_x$ (the last estimate makes use of the incompressibility condition $\nabla\cdot\mathbf{v} = 0$). The quantities α_2, α_3 are Leslie viscosity coefficients.[6] The coefficient α_2 is always negative, the sign of α_3 depends on the material. In our case $\alpha_3 > 0$. The torque contributions Γ_2 and Γ_3 along a vertical cut through the roll center ($x = 0$ in Fig. 6) are shown in Fig. 7 for our case with a rather large $|\alpha_2|$ and a comparatively large value of $\alpha_3/|\alpha_2| = 0.15$. Both torques are symmetric in z, which is consistent with the velocity field shown in Fig. 6. Γ_2 has extrema of opposite sign at the midplane ($z = 0$) and at the boundaries ($z = \pm d/2$) of the convection cell. Γ_3 has its maximum at $z = 0$, but is zero at $z = \pm d/2$. The torques Γ_2, Γ_3, which act in the same direction in most of the z-region, provide the positive feedback on the initial director distortion
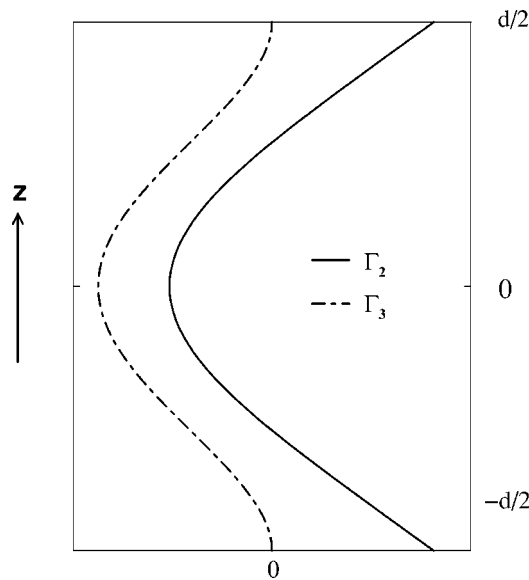
FIG. 7. Torque contributions Γ_2 and Γ_3 on a vertical cut through the center of a convection roll $x = 0$ in Fig. 6

$\delta\mathbf{n}$ necessary for the destabilization of the homeotropic director orientation $\mathbf{n}_0$. Counteracting stabilizing mechanisms are provided by the dielectric torque ($\epsilon_a > 0$) and the viscous damping of the flow. Thus there is a threshold voltage $U_0(q,\omega)$ ("neutral curve") above which patterns appear. Minimizing $U_0(q,\omega)$ with respect to q gives the critical voltage $U_c(\omega)$ and the critical wavenumber $q_c(\omega)$.

In Figs. 8(a) and 8(b) the experimental results for the threshold voltage U_c and the critical wave-number q_c are shown as functions of $\omega\tau_q$. The wavelength $\lambda_c = 2\pi/q_c$ is of the order of the cell thickness d as is the case in planar convection with conventional materials for frequences in the conductive range.

We note that in the usual nematics with $\sigma'_a - \epsilon'_a > 0$ the sign of the space charge in Fig. 6, and thus the flow direction, would be reversed. Consequently the hydrodynamic torque Γ_y would have to be reverted as well in order to reinforce the initial director fluctuation and to enable a direct transition to EC. Since $\Gamma_2 > 0$ is stabilizing in this case we would need a sufficiently strong negative Γ_3. This requires $\alpha_3 < 0$ and $q'^2 \sim |\alpha_2/\alpha_3| \gg 1$. It turns out that ϵ_a has to be near zero to enable the instability and that the threshold is rather large (see Refs. 24 and 8). Therefore the experimental situation for such materials is difficult.

In order to proceed to a quantitative description a linear stability analysis of the homeotropic ground state with the use of the full NHDE is needed. The resulting eigenvalue problem diagonalizes in Fourier space with respect to the horizontal coordinates $\mathbf{x} = (x,y)$ leading to modal solutions $\mathbf{V}(\mathbf{x},z,t) = e^{i\mathbf{q}\cdot\mathbf{x}}\bar{\mathbf{V}}(\mathbf{q},z,t)e^{\lambda(\mathbf{q})t}$. Here, $\bar{\mathbf{V}}(\mathbf{q},z,t)$ is periodic in time t with period $2\pi/\omega$. The symbolic vector $\mathbf{V} = (\phi,\mathbf{n},\mathbf{v})$ represents the field variables (electric potential, director, velocity). $\bar{\mathbf{V}}(\mathbf{q},z,t)$ is expanded with respect to the coordinate z into a complete set of functions that satisfy the correct rigid boundary conditions $\hat{\mathbf{n}} = \hat{\mathbf{z}}$, $v = 0$, $\phi = 0$ at the confining plates of the cell (Galerkin method). The periodic time de-
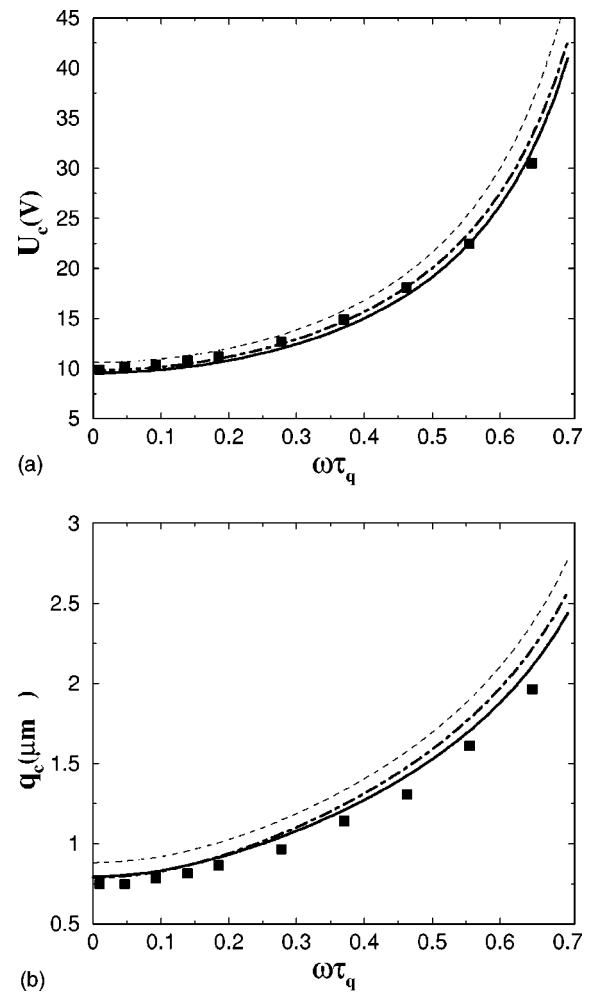

FIG. 8. Comparison between experimental (solid squares) and theoretical threshold voltage (a) and the corresponding critical wave number (b) vs dimensionless frequency. Solid line: rigorous Galerkin expansion; dot-dashed: two-mode formula [cf. Eq. (5)], dashed: one-mode formula [$M(q') \equiv 0$ in Eq. (5)].

pendence is captured by a Fourier expansion in time. Thus, the stability analysis amounts to a linear algebraic eigenvalue problem for the vector made up of the expansion coefficients. Consequently one obtains for fixed $\mathbf{q}$ a discrete set of eigenvalues $\lambda_i(\mathbf{q},U)$ and eigenvectors $\mathbf{V}_i(\mathbf{q},z,t)$ with the $\lambda_i, i = 1,2\cdots$ ordered according to decreasing real parts. The growth rate $\mathrm{Re}(\lambda_1(\mathbf{q},U))$ crosses zero at $U = U_0(q,\omega)$ ($q = |\mathbf{q}|$). In our case the bifurcation is stationary, i.e., $\mathrm{Im}[\lambda_1(\mathbf{q}_c,U_c)] = 0$.

As already mentioned some of the material parameters needed in the calculations are available from measurements: $\epsilon_\perp = 7.5\epsilon_0$, $\epsilon_a = 3.9\epsilon_0$, $\sigma_a/\sigma_\perp = -0.65$, and $K_{11} = 9.5 \times 10^{-12}N$.[10] The remaining ones were chosen in order to get a good fit for $U_c(\omega)$ and $q_c(\omega)$, which led to $K_{33}/K_{11} = 2.5$ for the ratio between the *bend* and *splay* elastic constants, and to $\alpha_1/|\alpha_2| = 3.5$, $\alpha_3/|\alpha_2| = 0.15$, $\eta_1/|\alpha_2| = 1.06$, and $\eta_2/|\alpha_2| = 0.21$ for the viscosity constants. Here the effective shear viscosities $\eta_1 = (-\alpha_2 + \alpha_4 + \alpha_5)/2$ and $\eta_2 = (\alpha_3 + \alpha_4 + \alpha_6)/2$ have been introduced. The positive and comparatively large values of α_1 and α_3 might appear surprising to specialists. However, they were necessary to obtain the correct low-frequency threshold and the strong

increase of q_c versus ω (in comparison to the conventional $\sigma_a > 0$ case). Also, as noted theoretically,[25] as well as experimentally using the material 4-n-octyl-4′-cyanobiphenyl (8CB),[26] and also in recent molecular dynamics simulations,[27] α_1 and α_3 are expected to become positive as in our case and in fact even to diverge near a second-order phase transition to a smectic phase.

In assessing the parameters we were guided by an analytic approximation for the neutral curve $U_0(q)$ [with the minimum $U_c = U_0(q_c)$] obtained from a Galerkin expansion with one z mode for $\mathbf{V}$ (e.g., $n_x \sim \sin(\pi z/d)$ and one time-Fourier mode. This leads to

$$U_0^2 = \frac{K_{33}\pi^2}{\epsilon_0 \epsilon_\perp} \frac{q'^2}{S_1}, \tag{5}$$

$$S_1 = \frac{1}{1 + k_1 q'^2}\left[I_h Q(q') \frac{\alpha_2 - \alpha_3 q'^2}{\eta_h(q')} - \epsilon_a^{\text{eff}}(q') \right],$$

$$\epsilon_a^{\text{eff}}(q')$$

$$= q^2 \epsilon_a' \frac{[\sigma(q')(1 + \sigma_a') + \omega'^2 \epsilon(q')(1 + \epsilon_a')](1 + q^2)}{\sigma(q')^2 + \omega'^2 \epsilon(q')^2},$$

$$\eta_h(q') = \eta_2 + (\eta_1 + \eta_2 + \alpha_1) I_1 q'^{-2} + \eta_1 \lambda_1^4 q'^{-4},$$

where $k_1 = K_{11}/K_{33}$, and $I_h = 0.97267$, $I_h' = 0.026056$, $I_1 = 1.24652$, $\lambda_1 = 1.50562$ are projection integrals. The results of the one-mode formula are included in Figs. 8(a) and 8(b) (dashed).

The one-mode formula, which captures the crucial mechanisms, has been given before[8,24] without reference to its applicability for $\sigma_a < 0$. Note also, that Eq. (5) can also be used to describe conventional EC with $\sigma_a > 0$ and planar alignment after some parameters have been interchanged ($\alpha_2 \leftrightarrow -\alpha_3, K_{11} \leftrightarrow K_{33}, \eta_1 \leftrightarrow \eta_2$). In the expressions for $S_1(q')$ one recognizes the EC mechanisms discussed above: The driving part proportional to $Q(q')(\alpha_2 - \alpha_3 q'^2)$ and stabilizing effects included in the effective shear viscosity $\eta_h(q')$ and the dielectric torque $\sim \epsilon_a^{\text{eff}}(q')$ (the complexity of this expression arises from the field distortion $-\nabla\phi$). Actually, in the homeotropic geometry, the effective viscosity is relatively large, which explains why the threshold is higher than in the planar geometry. The strong damping effect of the dielectric torque resulting from the large value of ϵ_a in our material is also responsible for the relatively low cutoff $\omega_{\text{cut}}\tau_q = 0.7$.

Finally we mention that an improved analytical threshold formula can be derived by including a second z-mode,[10] to get even nearer to the Galerkin curve (dashed-dot in Figs. 8(a) and 8(b)). This improvement is essential for materials where $\alpha_3/|\alpha_2|$ is very small; otherwise U_c is substantially overestimated.

IV. NONLINEAR RANGE

The theoretical methods for analyzing pattern forming instabilities in the nonlinear regime are discussed quite extensively in the literature (see, e.g., Refs. 8, 11, and 12). In order to describe stationary roll solutions and their stability starting from the NHDE all fields are expanded in Fourier modes in the horizontal directions $(x,y) = \mathbf{x}$ and in time t, as well as into Galerkin modes in z, similar to the previous section. The resulting nonlinear system of ordinary differential equations (ODE's) for the expansion coefficients yield the roll solutions. The stability problem can be treated analogously, after separating out Floquet exponents in $\mathbf{x}$ and t. In principle this approach can be extended to more complicated periodic solutions like squares, but the stability analysis based on the NHDE then becomes prohibitively complex.

Near threshold the calculations can be simplified in the framework of an extended weakly nonlinear analysis (see, e.g., Ref. 8, Sec. 3.5), which allows us to describe also additional slow variations of the patterns in time and space. At first the fields $\mathbf{V}$ are expressed in terms of the eigenvectors $\mathbf{V}_1(\mathbf{q},z,t)$ corresponding to the smallest growth rates of the linearized problem (see the previous section)

$$\mathbf{V}(\mathbf{x},z,t) = \sum_{\mathbf{q}} A(\mathbf{q},t)\mathbf{V}_1(\mathbf{q},z,t)\exp(i\mathbf{q}\mathbf{x}), \tag{6}$$

with $A(-\mathbf{q}) = A^*(\mathbf{q})$ because $\mathbf{V}$ is real. This representation is inserted into the NHDE, which are expanded up to cubic order in the amplitudes A. One thus arrives at the "order parameter equation" (see, e.g., Refs. 8, 11, and 28), which contains the standard four-wave-vector coupling of amplitudes A at cubic order. This approach allows an efficient study of rolls, squares, and hexagons and, in principle, of their stability near threshold.

In this way a perfect square pattern, which corresponds to two nonvanishing amplitudes for the orthogonal wave-vectors $\mathbf{q}_1 = (q,0)$, $\mathbf{q}_2 = (0,q)$ is constructed from the ansatz

$$A(\mathbf{q},t) = \bar{A}(\mathbf{q}_1,t)\delta(\mathbf{q} - \mathbf{q}_1) + \bar{B}(\mathbf{q}_2,t)\delta(\mathbf{q} - \mathbf{q}_2). \tag{7}$$

One arrives at

$$\tau_0 \partial_t \bar{A} = \sigma(q)\bar{A} - [\mu(q)|\bar{A}|^2 - \nu(q)|\bar{B}|^2]\bar{A}, \tag{8}$$

$$\tau_0 \partial_t \bar{B} = \sigma(q)\bar{B} - [\nu(q)|\bar{A}|^2 - \mu(q)|\bar{B}|^2]\bar{B},$$

with $\sigma(q) = \varepsilon - \xi^2(q - q_c)^2$. Here ε denotes the reduced control parameter $\varepsilon = (U^2 - U_c^2)/U_c^2$, ξ the coherence length and τ_0 the relaxation time. The functions $\mu(q), \nu(q)$ are found to be positive. For $\nu_c/\mu_c > 1$, where we use the definitions $\nu_c = \nu(q_c)$ and $\mu_c = \mu(q_c)$, there is a supercritical bifurcation to rolls [$\bar{B} \equiv 0$, $\bar{A}^2(q_c) \propto \varepsilon$ or equivalently $\bar{A} \equiv 0$, $\bar{B}^2 \propto \varepsilon$]. In the opposite case $\nu_c/\mu_c < 1$ rolls are unstable and stable squares with $\bar{A} = \bar{B}$ bifurcate.

Slow spatial modulations of the roll pattern with wave-vector $\mathbf{q}_c$ in the horizontal plane are described by an amplitude $A(\mathbf{x},t)$ which varies on a large scale $\gg \pi/q$ in space. $A(\mathbf{x},t)$ is obtained from $A(\mathbf{q})$ by a "shifted" Fourier transform

$$A(\mathbf{x},t) = \int_{D(\mathbf{q}_c)} d\mathbf{q}A(\mathbf{q},t)e^{i(\mathbf{q} - \mathbf{q}_c)\cdot\mathbf{x}}. \tag{9}$$

The integration is concentrated on a small area $D(\mathbf{q}_c)$ around the critical wave vector $\mathbf{q}_c = (q_c, 0)$ which we can choose in the x-direction.

Transforming the order parameter equation in this way back to position space one arrives at two coupled equations for A and a mean-flow velocity potential G

$$\tau_0 \partial_t A = \varepsilon(1 - e_3 2iq_c^{-1}\Box A)A + \xi^2\Box^2 A - \mu|A|^2 A$$
$$+ 2iq_c^{-1}[a_7|A|^2\Box A + a_8 A^2\Box^* A^* - A\partial_y G/2];$$

$$\Box = \left(\partial_x - \frac{i}{2q_c}\partial_y^2\right), \tag{10}$$

$$(\partial_x^2 + \partial_y^2)G = g_1\partial_y(A^*\Box A) + \text{c.c.} \tag{11}$$

These equations generalize the Newell–Whitehead equations [first line of Eq. (10) with $e_3 = 0$], where the locally rotation invariant combination of differential operators in $\Box$ has been introduced.[29] The linear term $\propto e_3$ yields to cubic order in $(q - q_c)$ a correction to the neutral curve $\varepsilon_N = \xi^2(q - q_c)^2[1 + 2e_3(q - q_c)]$. For $\varepsilon > \varepsilon_N$ roll solutions exist. The nonlinear terms $\propto a_7$, a_8 contribute to the ZZ instability (see below). The coupling to mean flow was first proposed in the context of RBC with intermediate Prandtl numbers.[30] In hydrodynamics, mean flow goes hand in hand with a pressure field, which satisfies a two-dimensional Poisson equation as is the case for G, see Eq. (11). Thus the mean flow (pressure) is long range and acts instantaneously.

In a rigorous derivation of Eqs. (10) and (11) at first for RBC[31] and later for planar nematic convection[32,33] a systematic method was presented to separate out the mean-flow contribution. Thus a smooth gradient expansion of the order parameter equation up to cubic order was ensured. In some cases a fairly large number of additional gradient terms had to be kept, to capture quantitatively all long-wave longitudinal and transverse instabilities near threshold. The same calculational scheme has now been applied to our system and we have determined all the necessary coefficients as a function of ω. We found excellent agreement between the full Galerkin method, the order parameter equations, and the amplitude equations near threshold in the weakly nonlinear regime $[0 \leq \varepsilon = (U^2 - U_c^2)/U_c^2 \ll 1]$.

With the material parameters determined in Sec. III we find a direct transition to squares at threshold for frequencies above $\omega_{\text{theo}}^* \tau_q \approx 0.60$, which correlates well with the experimentally observed crossover to squares at $\omega_{\text{exp}}^* \tau_q \approx 0.56$. In Fig. 9 we show a full stability diagram for rolls in the ϵ, q plane for a frequency slightly below ω_{theo}^*. Rolls with wavenumber q exist above the neutral curve $\varepsilon_N(q)$. Outside the region limited by the line $R(q)$ the rolls become unstable to growth of transverse rolls with wavenumber $q_{tr} \approx q_c$. Near onset $R(q)$ is easily obtained by considering $\bar{B}$ as the linear cross-roll perturbation of $\bar{A}$ in Eq. (8). One arrives at

$$R(q) = \frac{\xi^2(q - q_c)^2}{1 - \mu_c/\nu_c}. \tag{12}$$

To the left of line SQ, which meets the neutral curve at $(\varepsilon_{SQ}, q_{SQ})$, q is not contained in the band of q_{tr}. Thus the perturbations do not saturate to stable rectangles, but initiate a wavelength-changing process of the roll system. However, to the right of line SQ there exist destabilizing cross-roll processes with $q_{tr} = q$, which lead to amplitude-stable square
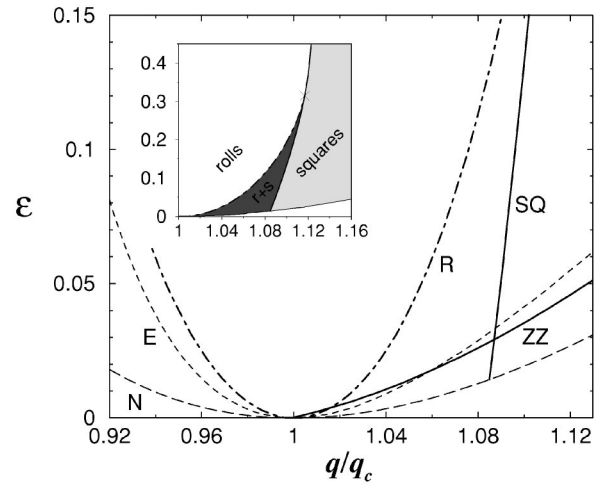

FIG. 9. Stability diagram below the transition frequency to squares at $\omega/\omega_{\text{theo}}^* = 0.82$. Above the neutral curve (N, dashed) the Eckhaus (E, thin dashed), and ZZ instability (ZZ, thick solid) are shown. The roll pattern is unstable against rectangles to the right of the R line and against squares to the right of the SQ line. The inset indicates the merging of the R with the SQ line (cross) at higher values of ϵ and the regions where one may expect rolls, rolls+squares (r+s), and squares.

patterns. For increasing ω the point $(\varepsilon_{SQ}, q_{SQ})$ moves down along the neutral curve, meets at ω_{theo}^* the threshold $(\varepsilon_{SQ} = 0, q_{SQ} = q_c)$ and moves again upward the neutral curve to the left for $\omega > \omega_{\text{theo}}^*$. The scenario can be understood very well on the basis of the coupled amplitude Eqs. (8) for the square patterns. It is obvious that amplitude-stable square solutions with wave-number q bifurcate if the condition $\nu(q)/\mu(q) < 1$ is fulfilled. The ratio $\nu(q)/\mu(q)$ turned out to be a monotonically increasing function of q for all ω in our case. Thus squares exist for all q above the lower limit q_{SQ} and for $\varepsilon > \varepsilon_{SQ} = \xi^2(q_c - q_{SQ})^2$, where q_{SQ} is determined by the condition $\nu(q_{SQ})/\mu(q_{SQ}) = 1$. Since on the other hand the ratio $\nu(q)/\mu(q)$ increases at fixed q with ω as well, it is obvious that q_{SQ} has to move to smaller values along the neutral curve when ω increases.

At onset the rolls are unstable against long wavelength ZZ modulations for all $\omega < \omega_{\text{theo}}^*$. Interestingly, the ZZ line which emerges linearly from the onset point $(\varepsilon = 0, q = q_c)$ is tilted strongly to the right. The slope can be easily calculated from the amplitude Eqs. (10) and (11) and is given by

$$\varepsilon_{ZZ}(q) = \frac{(q - q_c)}{q_c} \frac{\xi^2 q_c^2}{\dfrac{g_1 + a_7 - a_8}{\mu_c} + e_3}. \tag{13}$$

The contribution in the denominator due to the mean-flow contribution g_1 is about ten times larger than the other terms. Note that in the simple SHE the slope of the ZZ line is vertical. In contrast, in RBC the ZZ line tilts to the left (except for large Prandtl numbers, where it is essentially vertical).[1] In both cases the slopes result mainly from mean-flow effects, Eq. (11), but the coupling constant g_1 has opposite sign for the two systems. Thus, the mean flow generated by roll curvature tends to reinforce the curvature in EC, whereas it reduces it in RBC. The sign reversal in EC can be
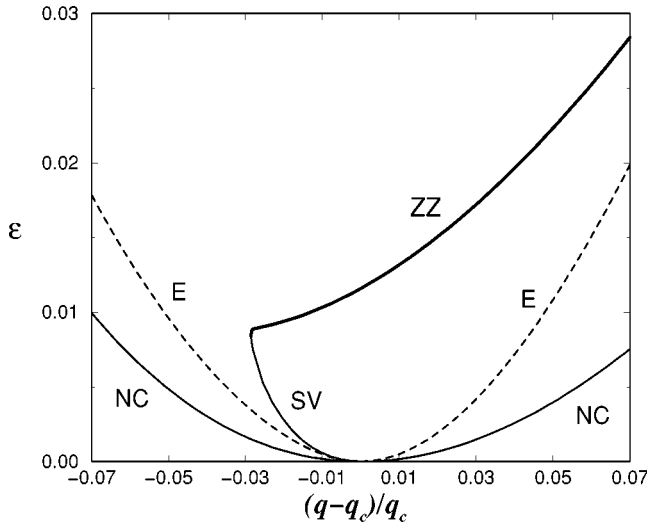
FIG. 10. Stability diagram at $\omega' = 0.3$ in the presence of a symmetry break-ing magnetic field $H_x = 0.9H_F$ with the Freedericks field $H_F = \pi/d\sqrt{k_{33}\chi_a}$. The ZZ line which would start at $q = q_c$ at zero magnetic field is shifted upward.

traced back to the influence of the Coulomb body force ap-pearing in the (modified) Navier–Stokes equation of the NHDE.

We have also studied the influence of a magnetic field in the x-direction that breaks the isotropy. Then the amplitude equations become slightly more complicated. In effect, the combinations of gradients $(\partial_x - i/2q_c \partial_y^2)$ typical for isotro-pic systems, splits into two independent contributions. A rep-resentative stability diagram is shown in Fig. 10. The ZZ line is shifted upwards and a stable roll regime appears.

The complex dynamic patterns shown in Figs. 1, 2, and 3 are not accessible to a Galerkin approach. Moreover, the full NHDE are at present not amenable to direct simulations. In this situation a model approach can be useful. Thus, we have constructed a suitable Swift–Hohenberg equation (SHE), which is a standard approach to model isotropic pattern-forming systems in the weakly nonlinear regime. Our SHE model reads

$$\tau_0 \partial_t \psi = \left[\varepsilon - \frac{\xi^2}{4q_c^2}(\Delta + q_c^2)^2 - \frac{e_3}{q_c^2}\varepsilon(\Delta + q_c^2) \right]\psi$$

$$- \left[\psi^3 + \frac{\gamma}{q_c^2}\psi(\nabla\psi)^2 \right] + \frac{\beta}{q_c^4}\partial_i[(\partial_i\psi)(\partial_j\psi)^2]$$

$$- \frac{1}{q_c^2}(\mathbf{U}\cdot\nabla)\psi, \tag{14}$$

$$(1 - c\Delta/q_c^2)\Delta G = -\frac{g_1}{2q_c^2}(\nabla(\Delta\psi)\times\nabla\psi)\cdot\hat{\mathbf{z}}, \tag{15}$$

with $\mathbf{U} = (\partial_y G, -\partial_x G)$, $c = 0.5$. Here $\psi(\mathbf{x}, t)$ portrays the pattern in the plane. This is a generalization of the "simple SHE" [34] obtained by setting $e_3 = \gamma = \beta = g_1 = 0$. The addi-tional cubic nonlinearities proportional to γ are well known from the literature to improve the description of RBC within the SH approximation.[11] The term $\sim\beta$ has been proposed to capture bifurcations to squares.[35] The description of the

mean flow $\mathbf{U}$ is also well established.[36] The term $\propto c$ is in-troduced to filter out short scale contributions to G.[37]

The coefficients of the SHE (14) and (15) are determined by mapping them for all ω onto the amplitude Eqs. (8) for squares and to Eqs. (10) and (11) for rolls with the use of the ansatz $\psi = \bar{A}e^{iqx} + \bar{B}e^{iqy} + $ c.c. We obtain $\mu(q) = 3 + 3\beta q^4 + \gamma q^2$ and $\nu(q) = 2(3 + \beta q^4 + \gamma q^2)$. For our material the cross coefficient ν_c/μ_c varies from 2.5 at $\omega = 0.1$ to 0.9 at $\omega = 0.7$ (it passes through 1 at ω_{theo}^*). This range can be covered in the SHE by varying continuously the coefficients β and γ. We fixed the so-far undetermined ratio γ/β by the requirement that the SHE should reproduce the values for q_{SQ}, ϵ_{SQ} of the NHDE, i.e., by the requirement $\nu(q_{\text{SQ}})/\mu(q_{\text{SQ}}) = 1$ as already discussed. The combination of a_7, a_8 which appear in the slope of ϵ_{ZZ} [see Eq. (13)] is given as $a_7 - a_8 = -3\beta$. As the final result of this mapping one obtains the parameters β, γ, g_1 as a function of ω, which can be parametrized as follows $\beta = -1.516 - 1.154\hat{\omega}^2 - 1.326\hat{\omega}^4$, $\gamma = -0.1318 + 3.048\hat{\omega}^2 - 1.092\hat{\omega}^4$, $g_1 = 36.3 + 51.32\hat{\omega}^2 + 411.51\hat{\omega}^4$ with $\hat{\omega} = \omega\tau_q$. It turns that the stabil-ity diagram obtained from the full SHE for rolls is practically indistinguishable from Fig. 9 up to $\varepsilon = 0.1$, which covers the experiments discussed in this paper.

For completeness some analytical results for the stability of squares $(\omega > \omega^*)$ are added. The ZZ-instability line cor-responding to modulations of one of the roll systems in squares is given by

$$\varepsilon_{\text{ZZ}}(q) = \frac{(q - q_c)}{q_c} \frac{\xi^2 q_c^2}{\frac{g_1 - 9\beta}{\mu_c + \nu_c} + e_3}. \tag{16}$$

Thus, it is obtained from the roll case Eq. (13) by the sub-stitution $a_7 - a_8 = -3\beta \rightarrow -9\beta$ and $\mu_c \rightarrow \mu_c + \nu_c$. Further-more, there exists a "rectangular" instability which involves coupled, symmetric modulations of both roll systems in squares.[19] It is operative outside of the parabola

$$\varepsilon_r = \frac{\xi^2(q - q_c)^2(3\mu_c + \nu_c)}{\mu_c - \nu_c}. \tag{17}$$

Note that the parabola collapses at ω^*.

V. SIMULATIONS AND DISCUSSION

In this chapter we describe and discuss results from nu-merical simulations of the SHE. Our main goal is to compare with the complex experimental patterns presented in Sec. II. Equations (14) and (15) have been solved using a standard pseudo-spectral code on a two-dimensional periodic domain, which covered up to $N = 30$ rolls with wavelength $\lambda_c = 2\pi/q_c$. The resolution was at least six gridpoints per λ_c. Thus, the relevant time scale is set by the horizontal diffu-sion time $t_H = N^2\tau_0$. Typically we started with random initial conditions and let the system evolve for at least $5t_H$.

The experimental ZZ patterns in Fig. 1(a) are well repro-duced by the simulation of the SHE immediately above threshold for ω well below ω_{theo}^* (ν_c/μ_c well above 1). We note that in Fig. 1 as in Figs. 2 and 3 the value of ϵ is smaller in the simulation than in the experiment. The larger experi-mental ϵ was needed to obtain sufficient contrast for the pic-

tures, but the pattern remains essentially the same in the experiments at the lower ε. The structure is reminiscent of patterns found in the simple SHE ($g_1 = 0$, corresponding to infinite Prandtl number Pr in RBC) at comparable ε, which appear only as transients[41] when starting a simulation from a ZZ unstable roll pattern ($q < q_c$). ZZ patterns are also observed significantly above threshold. In the latter case the q band widens and certain resonance processes involving modes with $q < q_c$ become active[38] which leads to frozen states. By contrast, in our case there is persistent slow dynamics. At intermediate Prandtl numbers in RBC (i.e., finite $g_1 \propto \mathrm{Pr}^{-1}$) sharp structures in the roll pattern are smoothed out by mean flow, whereas in our system grain boundaries remain sharp despite the strong mean flow. With increasing ω approaching ω^* at small ϵ we find a mixture of rolls and squares [R+S, see Fig. 2(b)] in good agreement with the experiments discussed in Sec. II, see Fig. 2(a). The undulated squares observed in experiments near onset [see Figs. 3(a) and 4(a)] are typically reproduced in the simulations for $\omega > \omega^*_{\mathrm{theo}}$, see Fig. 3(b).

Interestingly, for not too large ε ($\varepsilon \lesssim 0.022$ at $\omega/\omega^*_{\mathrm{theo}} = 1.16$), and then for large classes of initial conditions, all defects are pushed out in the simulations and one arrives at stationary soft squares with perfectly periodic undulations; see Fig. 4(b), which is a continuation of the run shown in Fig. 3(b). The final pattern represents a quasiperiodic solution of Eqs. (14) and (15) with an exact cubic symmetry, i.e., invariance under rotation by $\pi/2$. Stationary solutions of this type are indeed expected to exist quite generally. Since the modulations are of long wavelength, an approximate description is given by the nonlinear phase equation for the rectangular instability proposed in Ref. 19 with equal modulation wave numbers in the x and y direction. The quasiperiodic solutions are usually expected to be unstable representing saddle points which separate stable periodic solutions with different wave vectors. When the periodic solutions are destabilized, as is the case here, the situation may change. An analogous situation is known to arise in roll patterns undergoing the ZZ instability. In anisotropic systems one then has stable undulated roll structures in the regime where rolls are destabilized by the ZZ instability.[39] Similar effects have been predicted for isotropic systems.[40] For $\varepsilon \to 0$ the allowed modulation wavenumber should tend to zero. In this sense the quasiperiodic solutions do not bifurcate from the basic state in a direct way. For completeness we mention that in the immediate vicinity of the threshold (very small ε) the simulations tend to settle down to perfect squares, which is presumably an effect of the finite size suppressing the long-wave ZZ instability. This is not expected in the experiments because of the huge aspect ratio of the convection cells (several thousands of rolls).

The transition to hard squares occurring in the experiments with increasing ε are not captured appropriately by our SHE model. Instead, in the regime $\omega > \omega^*_{\mathrm{theo}}$, the simulations display with increasing ε increasingly disordered patterns characterized by patches of undulated squares separated by grain boundaries. On the other hand, at $\omega < \omega^*_{\mathrm{theo}}$, upon increase of ε above $\varepsilon_{\mathrm{QS}}$ the system tends to also settle in a state of rather well-ordered, undulated stationary squares

with wave-number $q > q_{\mathrm{SQ}}$, i.e., in the regime of amplitude-stable squares. Thus, interestingly, the mean flow, which increases with ϵ and destabilizes the roll pattern, seems to generate a selection process toward squares, which, if perfectly ordered, do not excite mean flow. We have checked that by reducing g_1 in Eq. (15) this crossover to squares is suppressed.

We suggest that the hard squares represent a superlattice where several groups of wave vectors interact to suppress the ZZ instability, a process easily missing in our SHE. Such superlattices, which often represent quasiperiodic structures, have been of considerable general interest recently.[42] They have been investigated experimentally in particular in the Faraday instability[43] in cells with aspect ratio up to about 50 and in oscillated RBC.[44]

VI. CONCLUSION

We have studied a model system for isotropic pattern formation, namely, a variant of EC in a nematic liquid crystal. Unlike other systems, the competition between rolls and squares can be systematically investigated at small amplitude in the same large-aspect ratio cell by merely changing the frequency of the applied ac voltage. Since the system is driven by an ac voltage it has an intrinsic reflection symmetry about the mid plane. Thus the quadratic resonance coupling leading to competing hexagons[15] is absent. In most cases the patterns near threshold exhibit a specific disorder with a slow dynamics. The disordered pattern is of the zigzag-type in the roll regime and undulated in the regime of squares. Interestingly, in simulations the undulations sometimes become completely regular, i.e., the soft squares settle into a static, spatially quasiperiodic attractor. In the experiments the dynamics of soft squares can become extremely slow and very nearly quasiperiodic, see Fig. 4.

The scenario originates in particular from the well-known transverse modulational ZZ instability, which is present in rolls as in squares, since it acts on each roll system individually (in contrast to hexagons, where the ZZ instability is suppressed).[19] The ZZ instability is here driven largely by the mean flow, which in our system acts quite differently than in RBC and has to be included already at threshold. Thus we have the unique case of a direct transition to a *stationary pattern* that is destabilized by long-wave instabilities leading to disorder or to an ordered, quasiperiodic pattern. Other experimentally accessible direct transitions to long-wave destabilized patterns involve Hopf bifurcations to *travelling waves*.[45,46] Alternatively, destabilization can be prompted by a short-wave instability, as in rotating RBC,[47] or by the presence of an additional Goldstone mode.[23] In all these cases the destabilization leads to disorder only. A particularly intriguing feature is that mean flow, which in RBC is responsible for the skewed varicose instability and spiral defect chaos[48] here leads to a very mild form of disorder or even to the generation of an unconventional ordered pattern.

In the future we plan to extract from weakly nonlinear theory a quantitative understanding of the soft square attractor, in particular its quasiperiodic manifestation. Also, a detailed description of the hard square pattern and the transition from soft to hard squares appears of interest. We expect simi-

lar phenomena in other systems provided the aspect ratio can be made comparably large. The ZZ instability may be replaced by some other long-wave destabilization, e.g., the skewed-varicose instability.

ACKNOWLEDGMENTS

[1] F. H. Busse, Rep. Prog. Phys. **41**, 1929 (1978).

[2] F. Simoni, *Nonlinear Optical Properties of Liquid Crystals* (World Scientific, Singapore, 1997); G. Demeter, Phys. Rev. E **61**, 6678 (2000); D. O. Krimer, G. Demeter, and L. Kramer, *ibid.* **66**, 031707 (2002).

[3] T. Börzsönyi, A. Buka, A. P. Krekhov, O. A. Scaldin, and L. Kramer, Phys. Rev. Lett. **84**, 1934 (2000).

[4] M. A. Scherer, G. Ahlers, F. Hörner, and I. Rehberg, Phys. Rev. Lett. **85**, 3754 (2000).

[5] *Pattern Formation in Liquid Crystals*, edited by A. Buka and L. Kramer (Springer-Verlag, New York, 1996).

[6] P. G. de Gennes and J. Prost, *The Physics of Liquid Crystals* (Clarendon, Oxford, 1993).

[7] L. Kramer and W. Pesch, in *Physical Properties of Nematic Liquid Crystals*, Vol. I, edited by D. A. Dunmur, A. Fukuda, and G. R. Luckhurst (EMIS Datareview No. 25, INSPEC, 2001), p. 441, and references therein.

[8] L. Kramer and W. Pesch, in *Pattern Formation in Liquid Crystals*, edited by A. Buka and L. Kramer (Springer-Verlag, New York, 1996), pp. 244 ff.

[9] W. Pesch and U. Behn, in *Evolution of Spontaneous Structures in Dissipative Continuous Systems*, edited by F. H. Busse and S. C. Mueller (Springer, New York, 1998).

[10] A. Buka, B. Dressel, W. Otowski, K. Camara, T. Toth-Katona, L. Kramer, J. Lindau, G. Pelzl, and W. Pesch, Phys. Rev. E **66**, 051713 (2002).

[11] M. C. Cross and P. C. Hohenberg, Rev. Mod. Phys. **65**, 851 (1993) and references therein.

[12] A. C. Newell, T. Passot, and J. Lega, Annu. Rev. Fluid Mech. **25**, 399 (1993).

[13] E. Bodenschatz, W. Pesch, and G. Ahlers, Annu. Rev. Fluid Mech. **32**, 709 (2000).

[14] F. H. Busse, J. Fluid Mech. **30**, 625 (1967).

[15] Squares at onset are observed in particular in RBC in the presence of bounding plates with finite heat conductivity, consistent with the theory (see, e.g., Ref. 16). The recently observed square patterns with a subsequent (secondary) transition to rolls have been found in Bénard–Marangoni convection (Ref. 17) and are at variance with the theoretical prediction of subcritical hexagons at threshold (Ref. 18). For other experimental systems see Ref. 19.

[16] P. Le Gal and V. Croquette, Phys. Fluids **31**, 3440 (1988).

[17] W. A. Tokaruk, T. C. A. Molteno, and S. W. Morris, Phys. Rev. Lett. **84**, 3590 (2000).

[18] A. Engel and J. B. Swift, Phys. Rev. E **62**, 6540 (2000).

[19] R. B. Hoyle, in *Time-Dependent Nonlinear Convection*, edited by P. A. Tyvand (Computational Mechanics, Southampton, 1998), p. 51; Physica D **67**, 198 (1993).

[20] A. Buka, B. Dressel, L. Kramer, and W. Pesch, Phys. Rev. Lett. (in press).

[21] U. Emmerling, S. Diele, H. Schmalfuss, J. Werner, H. Kresse, and J. Lindau, Macromol. Chem. Phys. **199**, 1529 (1998).

[22] Though not important in the present context, we give for completeness some information on the phase diagram. The following sequence of phases is identified: Cr 69 °C (S_x 66.5 °C) S_F 75 °C S_c 94 °C N 110 °C I. Here, I stands for the isotropic, N for the nematic, and S for the various smectic phases. Below 69 °C the substance crystallizes. Our measurements are performed quite near to S_c at 96 °C.

[23] A. G. Rossberg, A. Hertrich, L. Kramer, and W. Pesch, Phys. Rev. Lett. **76**, 4729 (1996).

[24] A. Hertrich, W. Decker, W. Pesch, and L. Kramer, J. Phys. (France) II **2**, 1915 (1992).

[25] F. Jähnig and F. Brochard, J. Phys. (Paris) **35**, 301 (1974).

[26] H. Kneppe, F. Schneider, and N. K. Sharma, J. Chem. Phys. **77**, 3203 (1981); Ber. Bunsenges. Phys. Chem. **85**, 784 (1981).

[27] L. Bennet and S. Hess, Phys. Rev. E **60**, 5561 (1999).

[28] H. Haken, *Synergetics* (Springer, New York, 1978).

[29] Though the number of independent parameters in Eqs. (10) and (11) can be reduced by a suitable rescaling, we have not done it to facilitate the later comparison with the SHE.

[30] E. Siggia and A. Zippelius, Phys. Rev. Lett. **47**, 835 (1991).

[31] W. Decker and W. Pesch, J. Phys. (France) II **4**, 419 (1994).

[32] M. Kaiser and W. Pesch, Phys. Rev. E **48**, 4510 (1993).

[33] E. Plaut and W. Pesch, Phys. Rev. E **59**, 1747 (1999).

[34] J. Swift and P. Hohenberg, Phys. Rev. A **15**, 319 (1977).

[35] C. J. Chapmann and M. E. R. Proctor, J. Fluid Mech. **101**, 759 (1980).

[36] P. Manneville, J. Phys. (Paris) **44**, 759 (1983).

[37] H. S. Greenside and W. M. Coughran, Phys. Rev. A **30**, 398 (1984).

[38] A. C. Newell, R. Passot, N. Ercolani, and R. Indik, J. Phys. (France) II **5**, 1863 (1995).

[39] E. Bodenschatz, M. Kaiser, L. Kramer, W. Pesch, A. Weber, and W. Zimmermann, in *New Trends in Nonlinear Dynamics and Pattern Formation Phenomena: The Geometry of Nonequilibrium, NATO Advanced Study Institute, Series B* 237, edited by P. Coullet and P. Huerre (Plenum, New York, 1990), p. 111.

[40] F. H. Busse and M. Auer, Phys. Rev. Lett. **72**, 3178 (1994).

[41] C. Bowman, T. Passot, M. Assenheimer, and A. C. Newell, Physica D **119**, 250 (1998).

[42] B. Dionne, M. Silber, and A. C. Skeldon, Nonlinearity **10**, 321 (1997).

[43] H. Arbell and J. Fineberg, Phys. Rev. E **65**, 036224 (2002).

[44] J. L. Rogers, O. Brausch, W. Pesch, and M. F. Schatz, Phys. Rev. Lett. **85**, 4281 (2000); Nonlinearity **16**, C1 (2003).

[45] P. Kolodner, S. Slimani, N. Aubry, and R. Lima, Physica D **85**, 165 (1995).

[46] M. Dennin, M. Treiber, L. Kramer, G. Ahlers, and D. Cannell, Phys. Rev. Lett. **76**, 319 (1996).

[47] Y. Hu, R. E. Ecke, and G. Ahlers, Phys. Rev. Lett. **74**, 5040 (1995).

[48] S. W. Morris, E. Bodenschatz, D. S. Cannell, and G. Ahlers, Phys. Rev. Lett. **71**, 2026 (1993).